Environment, Climate Change and Low Carbon Economy Programme

'Environment Programme'

European Economic Area (EEA) Financial Mechanism 2014-2021

A3 Report – Preliminary characterisation of formulations

31/01/2022

37_Call#2_Circular Construction in Energy-Efficient Modular Buildings

Accordingly, with the Articles 25.2.j) and 29.4 of the 'Applicants Guide for Financing of Projects Supported by Environment, Climate Change and Low Carbon Economy Programme'
https://www.eeagrants.gov.pt/media/2994/applicants-guide-for-financing-eea-grants_environment-projects_28112019.pdf

1. Introduction

This report presents the actions developed during activity A3 – Preliminary characterisation of formulations, which were concluded between March 2021 and January 2023.

This activity was divided into eight actions carried out by all the partners:

- Preliminary formulations
- Optimisation of volumetric mass;
- Nanoparticles fabrication;
- Nanostructural analysis;
- Nanoparticles incorporation;
- Durability assessment;
- Environmental assessment;
- Microstructural analysis.

2. Preliminary formulations

To better understand the potential of each waste to participate in the production of the pastes that will constitute the core of the panels, several formulations, combining the several wastes available, were prepared and submitted to uniaxial compressive strength (UCS) testing. The compressive strength was chosen as the evaluation parameter at this early stage of the A3

since it is regarded as a simple and easy procedure capable of giving important information regarding the reactivity of the wastes. As such, a total of 109 different mixtures (42 included nanoparticles) for the core material and 17 more formulations for the external rendering mortar (2 incorporated nanoparticles). This first analysis stage allowed for defining the ideal conditions and compositions for the next development phase.

Seven weight ratios between the secondary wastes (fly ash and marble and granite residues) and 3 weight ratios between the primary wastes (ceramic and glass) were defined and tested. The remaining 4 primary wastes were not tested at this stage since they are not expected to perform adequately in a precursor role. Instead, they were included as a filler or as gas generators (to form the pore structure of the final pastes) in the A3.2.

2.1. Curing temperature and humidity

Two different curing environments – 40ºC / 90% relative humidity and 85ºC at dry conditions – were considered. Each action included the whole production of a particular set of three prismatic specimens, its curing for 7 days, and the subsequent mechanical tests (3 flexural tests and 6 compressive tests).

2.2. Hydroxide molality

The analysis of 2 different molalities for the hydroxide (5 and 8 molal) was considered. Each action included the full production of a particular set of three prismatic specimens, its curing for 7 days, and the subsequent mechanical tests (3 flexural tests and 6 compressive tests).

2.3. Silicate incorporation

Four different silicate contents were added to two selected mixtures from the previous stages. Each action included the full production of a particular set of three prismatic specimens, its curing for 7 days, and the subsequent mechanical tests (3 flexural tests and 6 compressive tests).

The mechanical resistance to compression and flexion at the age of 7 days were the properties chosen to monitor the effects of changes in composition and curing conditions of the different compositions made. The information obtained served as a reference for selecting some of the compositions that showed the best mechanical performance, which were reformulated to improve their mechanical behaviour by adding SS in the alkaline solution formulation. For each composition, the specimens made to evaluate the mechanical properties were prismatic

specimens of 40x40x160 mm. Table 1 shows the summary of each of the synthesised preliminary mixes.

Table 1: Composition of synthesised premixes.

Mixture	Mass (g)	Precursor						S / L
		Marble	Granite	Fly Ash	Slag	Ceramic	Glass	
1	1200	70%		30%				0.35
2	1200	50%		50%				0.35
3	1200	30%		70%				0.35
4	1200	70%	30%					0.39
5	1200	50%	50%					0.39
6	1200	30%	70%					0.39
7	1200			100%				0.35
8	1200	70%		30%				0.35
9	1200	50%		50%				0.35
10	1200	30%		70%				0.35
11	1200	70%	30%					0.40
12	1200	50%	50%					0.42
13	1200	30%	70%					0.41
14	1200			100%				0.35
15	1200					30%	70%	0.37
16	1200					50%	50%	0.37
17	1200					70%	30%	0.37
18	1200					30%	70%	0.35
19	1200					50%	50%	0.35
20	1200					70%	30%	0.35

Regarding temperature and humidity results, the conditions carried out in the preliminary mixtures were carried out for the formulations with Marble and Granite, using two types of thermal curing: 40°C and 90% relative humidity and 85°C and 0% humidity relative. **BR** For mixtures containing ceramic and glass waste, curing temperatures of 65 °C and 85 °C were used, both with relative humidity of 0%. Table 2 shows the summary of the curing conditions of the preliminary mixes and table 5 shows the mechanical strength results obtained at 7 days of age.

Table 2: Curing conditions.

Mixture	Cure (stove)		
	Time (h)	Temperature	Humidity
1	24	40	90%
2	24	40	90%

3	24	40	90%
4	24	40	90%
5	24	40	90%
6	24	40	90%
7	24	40	90%
8	20	85	0%
9	20	85	0%
10	20	85	0%
11	20	85	0%
12	20	85	0%
13	20	85	0%
14	20	85	0%
15	20	65	0%
16	20	65	0%
17	20	65	0%
18	20	85	0%
19	20	85	0%
20	20	85	0%

Table 3: Mechanical resistance at 7 days.

Mixture	Results (MPa)	
	Flexure	Compression
1	0.7	1.7
2	0.6	1.8
3	0.6	1.8
4	0.2	0.6
5	0.2	0.5
6	0.2	0.4
7	0.2	0.3
8	1.4	9.0
9	1.8	11.6
10	1.9	10.2
11	1.7	5.8
12	1.8	6.0
13	1.4	5.0
14	0.4	2.5
15	0.44	0.70
16	0.24	0.64
17	0.14	0.59
18	0.55	0.95

19	0.73	1.39
20	1.28	1.55

The results showed that the compositions that used fly ash as a complementary precursor and were additionally cured at a temperature of 85°C presented the best mechanical results at 7 days. This behavior is very classic in compositions containing fly ash since when low-calcium fly ash is alkaline activated, an external activation energy is necessary to start the dissolution processes, consequently leading to the generation of cementitious gel as a product (main reaction which is responsible for agglomerating the particles of the alkaline activated mixture). It should be noted that these curing conditions and the mechanical resistance in this type of system are not directly proportional since, at some point, an excess or a lack of humidity in the alkaline-activated system can play to the detriment of the formation of reaction products and therefore generate luting agents with low mechanical resistance.

3. Optimisation of volumetric mass

Two stages are dedicated to developing the high-pore pastes, followed by one stage for incorporating the four primary wastes (wood, EPS, plastic and slag). Based on the literature review on the subject, different reagents will be tested. The development of a paste with only slag (precursor) activated by sodium hydroxide to evaluate the possibility of a direct porous mixture will also be included.

- Single slag activation: Production of a minimum of 4 'key-pastes' from slag and activator alone, and parametric analysis of the time of rest before oven curing, solid/liquid ratio and silicate content.
- Incorporation of pore-inducing agents in complex pastes: Incorporation of slag or aluminum powder as chemical pore-inducing agents in pastes selected from A3.1, and parametric analysis of time of rest before oven curing, solid/liquid ratio and silicate content.
- Incorporation of wood, EPS and plastic in complex pastes: Incorporation of six different contents of wood or EPS as physical pore-inducing agents in pastes selected from the first two stages.

Each action included the full production of a particular set of three prismatic specimens, its curing for 24h, and the mechanical tests (3 flexural tests and 6 compressive tests). Also included

is the rheology assessment (Vicat Apparatus), the volumetric mass density (by direct and precise weighting and measurement of the prismatic specimens), the pH measurement of the fresh paste and the measurement of type P seismic wave velocity through each paste, after curing is complete (this will yield the dynamic elastic modulus of the cured paste, immediately prior the first mechanical testing). Samples will be taken for the Microstructure Analysis during A3.6, frozen in acetone or equivalent to halt the reactions, and stored isolated from any moisture or air contact.

4. Nanoparticles fabrication

SiO_2 and Al_2O_3 nanoparticles were fabricated using a planetary ball-milling tool. Typically, about 20 g powders were milled for 5 hours. A 250 ml tungsten carbide vial and 100 tungsten carbide balls of different dimensions were used as milling media. The weight ratio of ball-to-powder was about 40:1 and the milling speed was 200 rpm. To prevent excessive cold-welding, 3 wt.% of stearic acid, which functioned as a process control agent (PCA), was added to each bowl. The resulting particles were washed several times with 4 mol/L HCl in an ultrasonic bath.

5. Nanoparticles analysis

5.1. Morphological and structural analysis

The morphologies and size distribution of the nanoparticles were observed in a High-Resolution Environmental Scanning Electron Microscope (SEM) with X-Ray Microanalysis and Electron Backscattered Diffraction (EBSD) analysis (Quanta 400 FEG ESEM/ EDAX Genesis X4M) using an acceleration voltage of 25 kV. The SEM images were taken at 2000×, 20000×, 50000× and 100000× magnifications. The Scanning Electron Microscopy images of the nanoparticles are displayed in Figure 1, showing that for SiO_2 nanoparticles, some agglomeration is observed with spherical and homogenous morphology for the smaller size (60-70 nm). As for SiO_2 1000 nm particles are observed with irregular and large distribution of sizes. The Al_2O_3 80 nm particles micrograph shows highly porous with highly agglomerate size, as presented in Figure 2. For the larger size, similarly to the SiO_2 particles, a large distribution of sizes is observed, being mixed in the form of nanorods and irregular size and shape. Concerning the ZrO_2, Figure 3 shows that the particles present high agglomeration for the 40 nm size. As for the 800 nm, the ZrO_2 particles appear spherical and homogeneous. For the TiO_2 images (Figure 4), it is possible to observe that the 30 nm, 50 nm and <100 nm nanoparticles present cubic and homogeneous morphology. For

the 500 nm size, the nanoparticles show a spherical morphology, while the 5000 nm nanoparticles have an irregular and heterogeneous morphology and a large distribution.

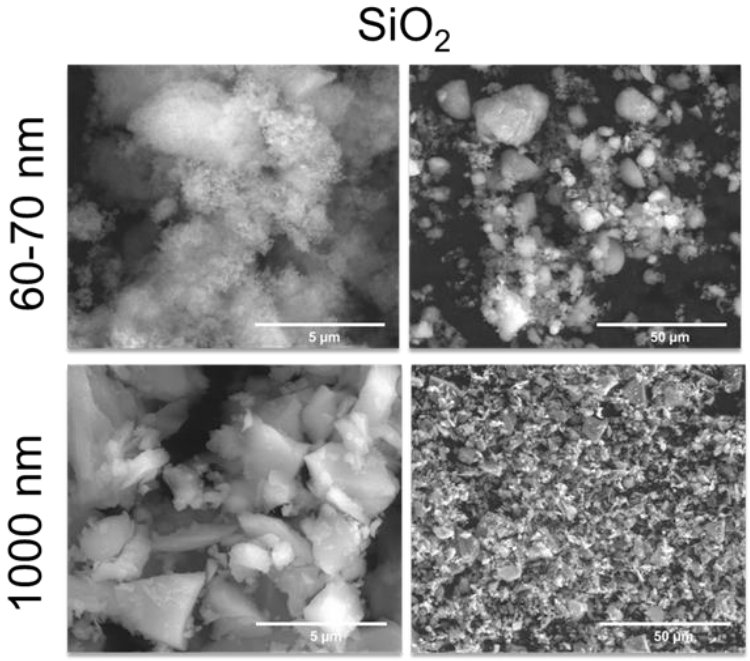

Figure 1: Scanning electron microscopy (SEM) images of SiO_2 60-70 nm and 1000 nm. Scales bars: 5 and 50 µm.

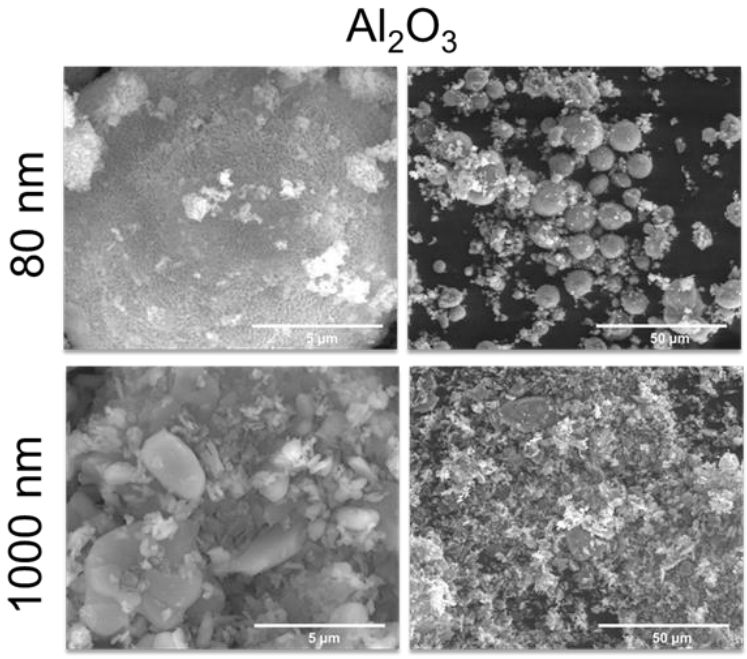

Figure 2: Scanning electron microscopy (SEM) images of Al_2O_3 80 nm and 1000 nm. Scales bars: 5 and 50 µm.

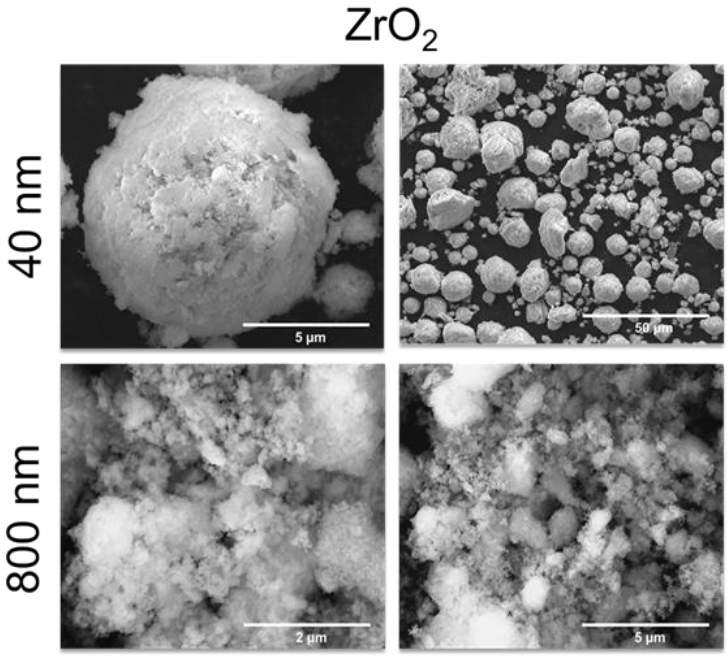

Figure 3: Scanning electron microscopy (SEM) images of ZrO_2 40 nm and 800 nm. Scales bars: 2, 5 and 50 µm.

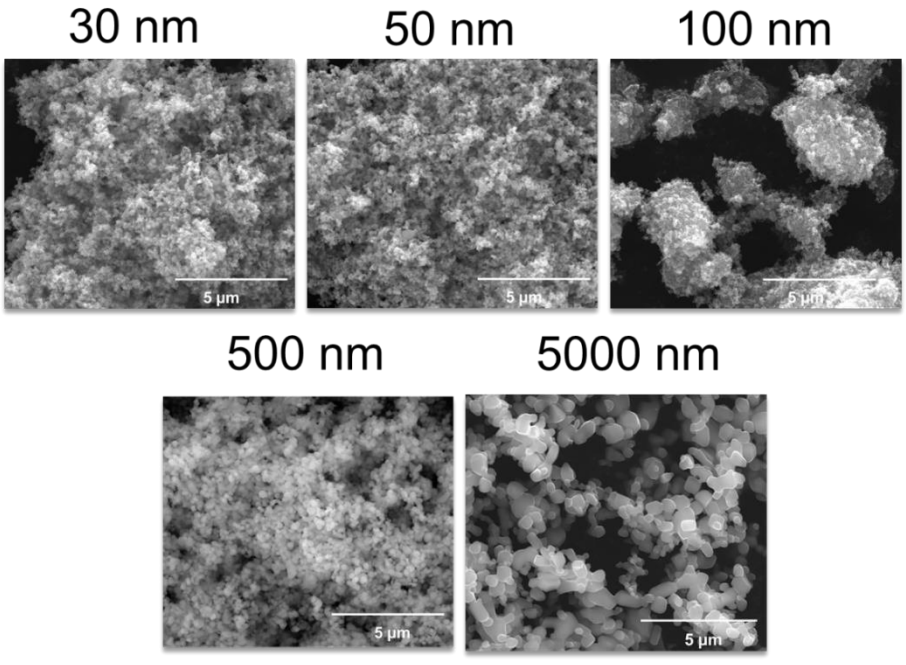

Figure 4: Scanning electron microscopy (SEM) images of TiO_2 30, 50, 100, 500 and 5000 nm. Scales bars: 5 µm.

Structural characterisation was carried out by X-ray diffraction (Rigaku SmartLab; 45 kV and 200 mA) at room temperature using Cu-Kα radiation (1.540593 Å) and the Bragg–Brentano θ/2θ geometry in the 10°-90º 2θ range, with a step of 0.02° and a scan rate of 12° min^{-1}. This

system offers high-resolution data via a Johansson Ge $K_{\alpha 1}$ monochromator. The X-ray diffraction (XRD) patterns of the nanoparticles are presented in Figure 5**.** The intense and sharp peaks found in the diffraction patterns reveal the crystalline nature of the powders.

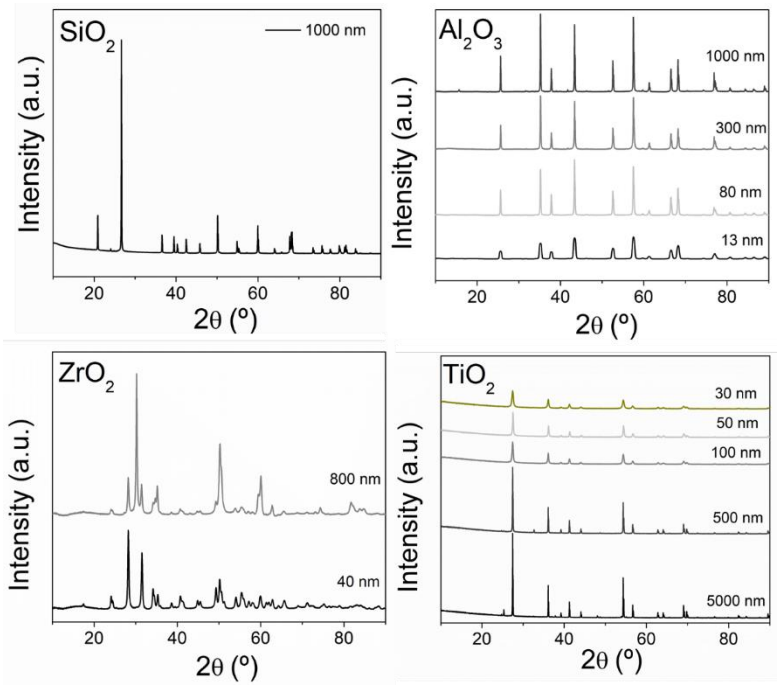

Figure 5: XRD patterns of the nanoparticles used in the study.

5.2. Optical assessment and band gap calculation

When the sunlight is absorbed or reflected, several electronic transitions may occur. Band gap calculation is one possibility to predict and study the optical properties of a nanomaterial. As such, to measure the reflectance and to calculate the optical band gap energy, the nanoparticles were co-pressed axially into a layered pellet at 28 MPa for 2 minutes, as shown in Figure 6.

Figure 6: Nanoparticle pellet preparation.

A modular spectrophotometer [two spectrophotometers coupled with different wavelengths: FLAME-T (UV-VIS) and FLAME-NIR (NIR)] from Ocean Optics was used to assess the

optical properties of the nanoparticles in the 200-1650 nm range. Each sample was measured three times and averaged at distinct locations to calculate the spectral reflectance based on Table X2.1 100 ordinates Direct Normal Irradiance A.M. 1.5 of ASTM G173 (ASTM G173, 2020) and following the procedure established in ASTM E903 (ASTM E903, 2020). The solar reflectance (SR) was calculated based on:

$$\mathbf{SR} = \frac{\int_{280}^{1650} \mathbf{RI}(\boldsymbol{\lambda})\mathbf{d}\boldsymbol{\lambda}}{\int_{280}^{1650} \boldsymbol{I}(\boldsymbol{\lambda})\boldsymbol{d}\boldsymbol{\lambda}}, \quad (1)$$

while the near-infrared (SR_{NIR}) was calculated using the following:

$$\mathrm{SR_{NIR}} = \frac{\int_{700}^{1650} \mathrm{RI}(\lambda)\mathrm{d}\lambda}{\int_{700}^{1650} \mathrm{I}(\lambda)\mathrm{d}\lambda} \quad (2)$$

The reflectance data of the nanoparticles was then converted in the Kubelka Munk function F(R), which is one of the most used methods to determine the optical band gap:

$$\mathrm{F\,(R)} = \frac{\alpha}{\mathrm{s}} = \frac{(1-\mathrm{R}_\infty)^2}{2\mathrm{R}_\infty} \quad (3)$$

where α is the absorption coefficient, s the effective scattering coefficient, and R_∞ the reflectance at an infinite thickness. This method can be applied to semiconducting materials that do not absorb light in the visible region. The results from the reflectance assessment and calculation of the band gap are represented in Figure 7. It is evident that these nanomaterials have a wide band of energy, which means that it is expected that they will reflect light. The slight differences observed between the values are attributed to the particle size and crystalline phase. Taking into consideration the literature, the values are in good agreement. Regarding the reflectance of the pellets, it is possible to observe that they exhibit different behaviour for varied sizes within the same group of nanomaterials. The total and near-IR reflectance for these materials is more significant than 0.65 (considered reflective material). Such data corroborate the results obtained for the band energy of nanomaterials.

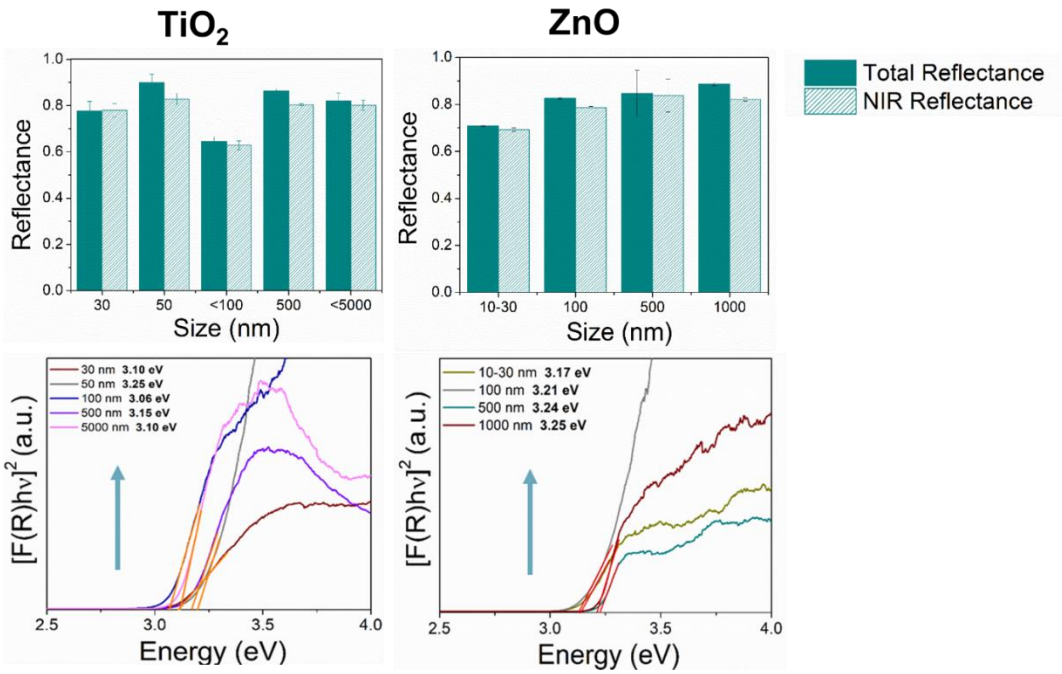

Figure 7: Calculated total and NIR Reflectance and representation of $[F(R)\ hv]^2$ versus hv for TiO_2 and ZnO nanoparticles used to incorporate the finishing coatings.

Such results can lead to new formulations of solar reflective coatings able to reduce the overall cooling load, particularly in warm climates with high cooling demands. The nanoparticles selected to incorporate the finishing coating of the SIP panels were TiO_2 30 nm, ZnO 500 nm and SiO_2 60-70 nm.

6. Nanoparticles incorporation

6.1. Formulations of external and core pastes

Incorporation of SiO_2 (60-70 and 1000 nm), Al_2O_3 (80 and 1000nm) and ZrO_2 (40 and 800 nm) with different sizes in the formulations of external and core pastes was performed. The mixtures were alkali-activated with sodium hydroxide (NaOH, 3M) and sodium silicate (ratio of NaOH/silicate was 0.3). The solid/liquid ratio was to provide mechanical strength. After the activator addition, the specimens were cured in controlled ambient (85ºC, 40% HR) for about 20h (Figure 8).

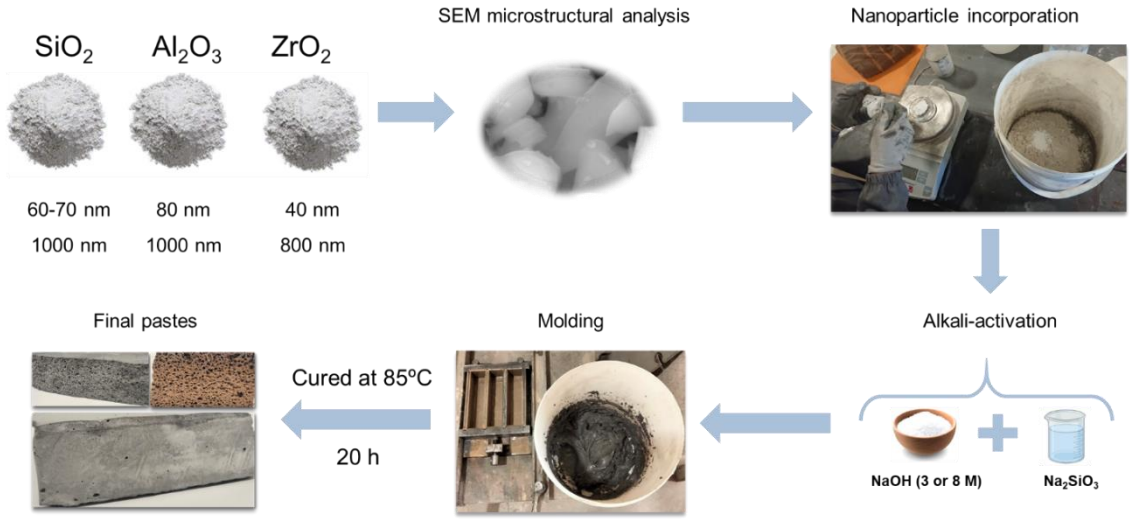

Figure 8: Experimental methodology applied in the production of alkaline-activated mixtures.

Three formulations were selected, and three solutions were created at dosages of 0.5%, 1% and 2 wt% nanoparticles (Table 4); each was gradually added to the dry powders.

Table 4: Selected formulations to incorporate nanoparticles.

Mixture	Marble	Fly Ash	Slag	PU	Timber	Powdered Aluminum	S/L	H/S
29	50%	50%	---	---	---	---	0.41	1.00
47	---	90%	---	5%	5%	0.1%	0.60	0.30
57	24%	24%	46%	---	---	---	1.00	0.50

The nanoparticle-doped formulations were subjected to an experimental campaign that included compressive and flexure resistance, determination of density and workability. The obtained results are presented in Figure 9, Figure 10 and Figure 11. Formulation 29, according to Figure 9, presents a non-monotonous behaviour of density, compression and flexure with the incorporation of nanoparticles. The minimum values for the three parameters are between 0.5% and 1% nanoparticle concentration.

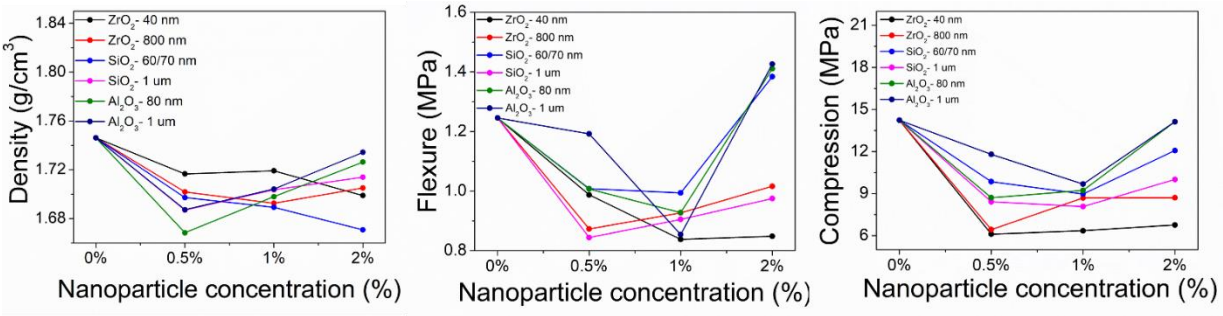

Figure 9: Nanoparticles incorporation in mixture 29.

Similarly to mixture 29, formulation 57 presents a non-monotonous behaviour of density, compression and flexure with the nanoparticle incorporation. The density typically lowers at 0.5% concentration. On the contrary, the compression increases with nanoparticle concentration, as shown in Figure 10.

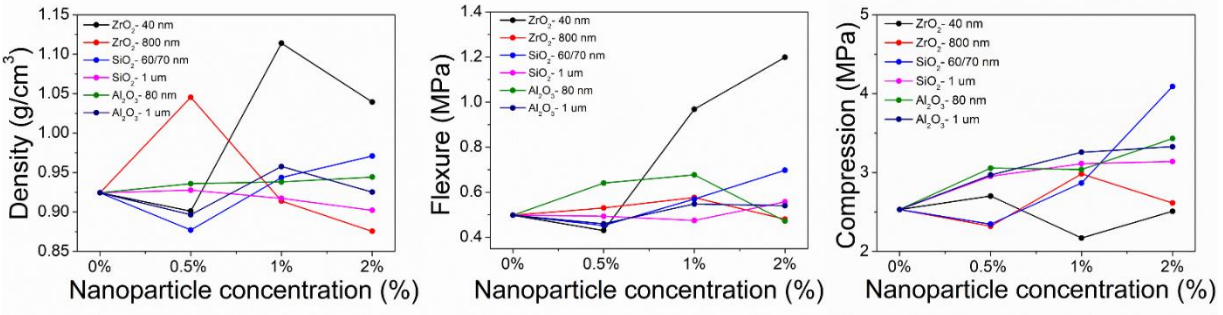

Figure 10: Nanoparticles incorporation in mixture 57.

Considering the previous results obtained for the mechanical strength, the formulation selected to produce the SIP panel was doped with the smaller sizes of SiO_2 and Al_2O_3 at a concentration of 0.5% (w/w). In Figure 11, it is evident that the SiO_2 decreases density and flexure and promotes an increase in compression resistance. Regarding Al_2O_3, the opposite behaviours occur.

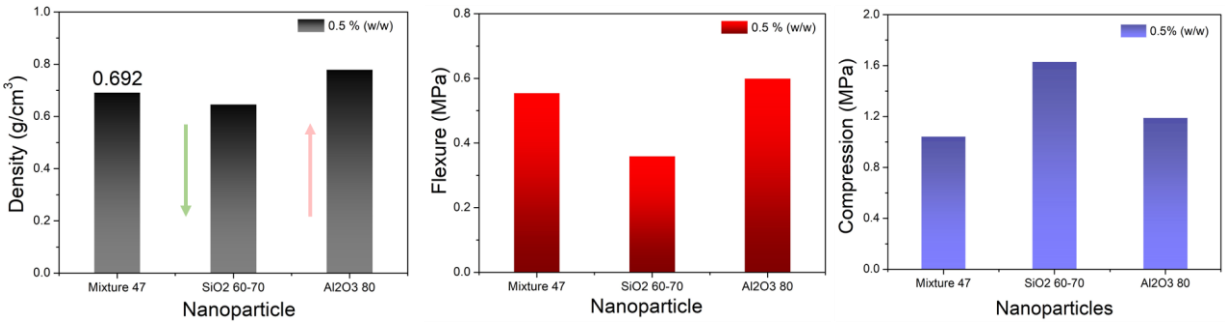

Figure 11: Nanoparticles incorporation in mixture 47 at 0.5% concentration.

The results obtained allowed the definition of the best formulations based on density and mechanical performance, which were incorporated into the live-scale panels.

6.2. Incorporation in black acrylic paint to finish the panels

To study the effect of reflective nanoparticles in the finishing layer of the SIP panels, a commercial aqueous acrylic paint with amorphous carbon as the black pigment was used. According to the technical documents, this paint is suitable for exterior coating in any climate. The study consisted of optimising the formulations with the commercial paint doped with reflective nanomaterials, such as TiO_2 (30 nm), ZnO (500 nm) and SiO_2 (60-70nm). The nanomaterials were combined to obtain different concentrations (1 to 20% w/w), in acrylic substrates. The objective was to understand their intrinsic properties, such as size, crystalline phase and morphology, on the paint performance in the UV-Vis and NIR region. The visual appearance of the samples can be seen in Figure 12.

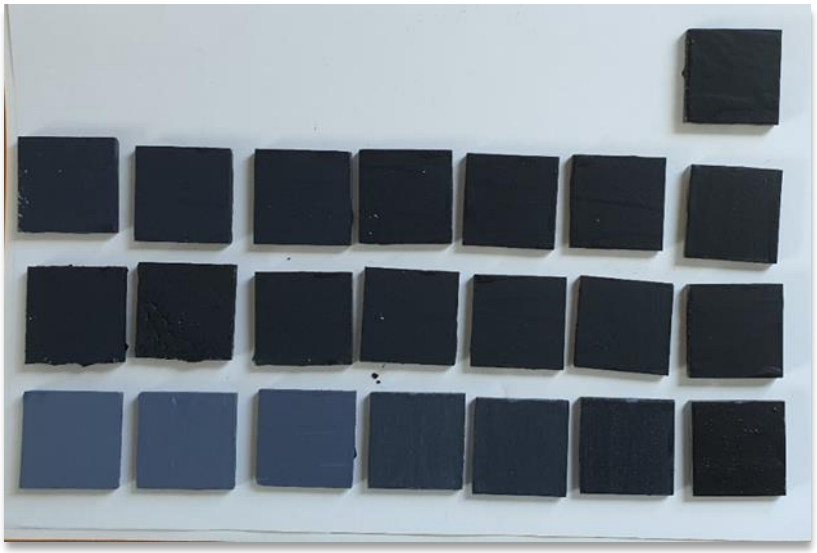

Figure 12: Incorporation of TiO_2, SiO_2 and ZnO in the acrylic paint, in acrylic substrates.

After producing the samples, several reflectance and colourimetric measurements were carried out, using the modular spectrophotometer to perform a comparative analysis between the several samples to choose the best nanoparticle with the adequate size and concentration that demonstrates the most balanced results, i.e., enhanced reflectance with similar visual aesthetic. The results of the solar reflectance measurements are shown in Figure 13 arranged by nanoparticle size and respective percentages mixed in the paint. From the results, it is verified

that the incorporation of nanoparticles in the acrylic paint, in general, causes an increase in total and NIR reflectance.

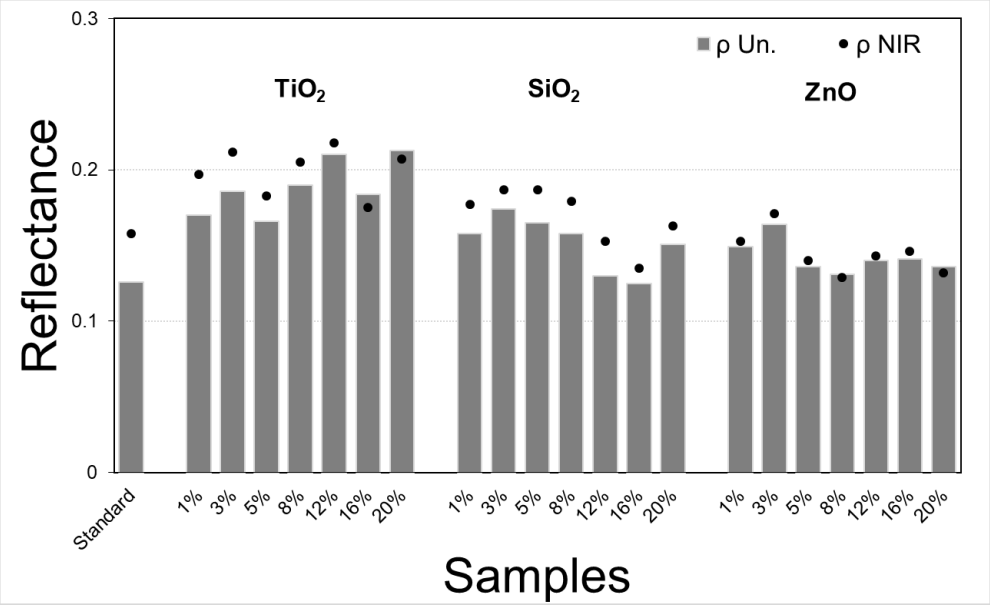

Figure 13: Calculated reflectance for the acrylic paint doped with nanoparticles in acrylic substrates.

One of the main goals of this study was to improve the reflectance of the paint without excessively changing its colour. The colour difference calculation (Eq.4) lets us understand whether the samples' changes are similar.

$$\Delta E^*_{ab} = [(\Delta L^*)^2 + (\Delta a^*)^2 + (\Delta b^*)^2]^{1/2} \quad (4)$$

where ΔL*= L1* – L2* is the difference in lightness (with ΔL*>0 indicating lighter material), Δa*= a1* - a2* is the difference between red and green (with Δa*>0 indicating shades redder) and Δb*=b1* - b2* is the difference between yellow and blue (with Δb*>0 indicating more yellowish tones). For human eyes, the differences in perceivable colour can be classified into three main categories:

- ΔE> 3: very perceptible;
- 1.5< ΔE< 3: perceptible
- ΔE<3: almost imperceptible.

Although the difference between 1.5 and 3 is perceptible, it is widely accepted in the coating industry. An equally important index that completes the colour characterisation is the Yellowness Index (YI), which quantifies the degradation process by light or other agents. The

index variation expresses the degradation in module. Therefore, the higher the YI, the higher the sample's degradation. This parameter can be essential to evaluate samples after being submitted to an accelerated ageing cycle or natural weathering exposure. Such index can be quantified using the following equation 5. We performed the colour analysis comprising the colour difference and yellowness index, displayed in Figure 14.

$$YI = \frac{142.85\ b^*}{L^*} \quad (5)$$

Regarding the colour variation, the samples with the best behaviour were the SiO_2 60-70 nm, followed by ZnO nanoparticles. The TiO_2 nanomaterials incorporation presented the highest colour change.

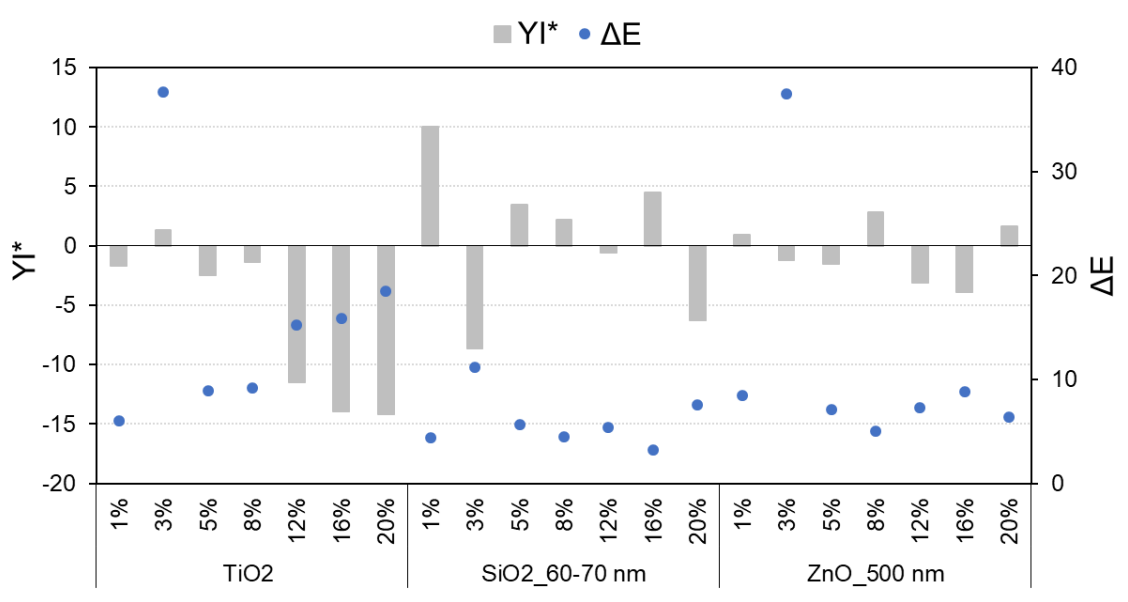

Figure 14: Color change in acrylic paint-doped samples' TiO_2, SiO_2 and ZnO.

The nanoparticles at 8% concentration were considered colour-matched and suitable candidates to incorporate the finishing layer of the SIP panels, maintaining the balance by enhancing the reflectance without significantly modifying its colour.

Two formulations (see Table 5), one for the external rendering panel and the other for the ventilated façade panel mortar, were selected to study the effect of introducing nanoparticles in the finishing coating.

Table 5: Formulations selected for the external rendering and the ventilated façade panel.

System	Mixture	Fly Ash	CDW	PU	Timber	Powdered Aluminum	S/L
Mortar for exterior SIP panel	A7	50%	50%	---	---	---	0.32
Mortar for ventilated facade panel	47	90%	---	5%	5%	0.1%	0.60

Four samples for each system were produced, as illustrated in Figure 15. Considering the preliminary studies, the selected nanoparticles were incorporated into the acrylic paint at 8% concentration.

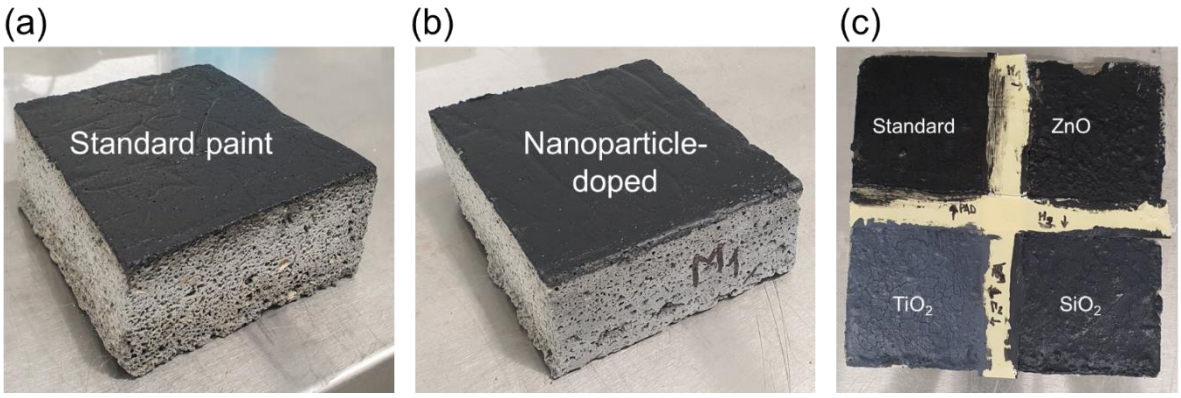

Figure 15: SIP mortar for ventilated facade panel samples coated with (a) commercial black acrylic paint and (b) SiO2-doped black acrylic paint; (c) mortar for exterior SIP panel with commercial black acrylic paint non-doped and doped with reflective nanoparticles.

To measure the reflectance, we follow the same standard procedure as previously, which allows for evaluating the NIR-reflectance behaviour. The results of reflectance (Figure 16) for each mortar shows that the reflectance is similar for the same concentration of nanoparticles (8%), with acrylic paint applied as finishing coating.

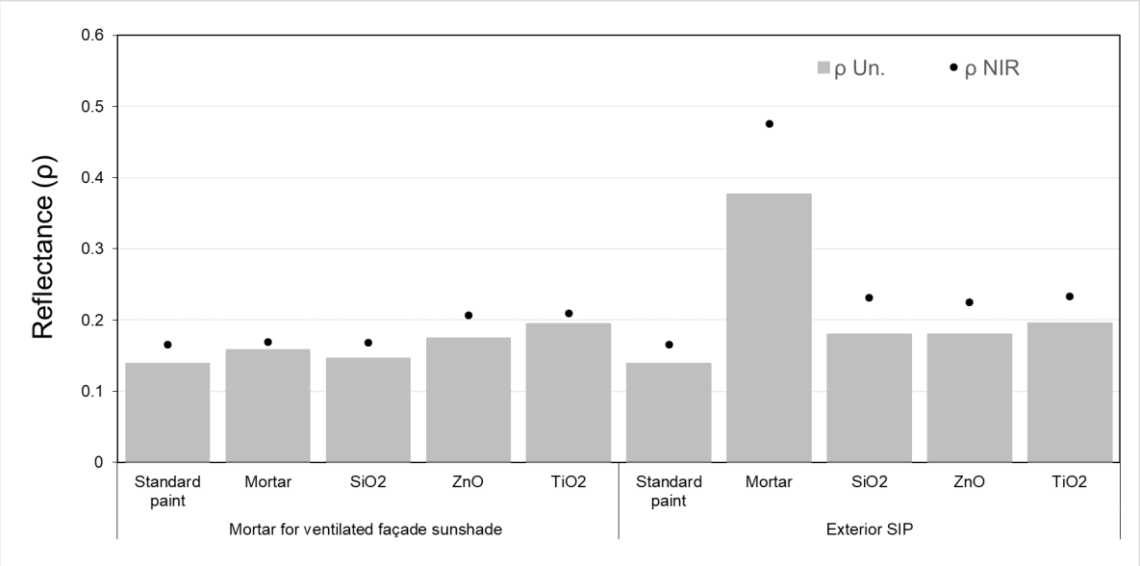

Figure 16: Reflectance results for samples with acrylic paint in the two SIP panel systems.

It should be noted that the validity of the results for the exterior SIP plaster is not completely acceptable due to the high fracture of the coating when applied directly to the mortar. As such, the valid results refer to the mortar for the ventilated façade panel. The analysis of Figure 17 allows us to confirm the influence of the nanoparticles in the acrylic paint, increasing the reflectance. Thus, it is observed that regardless of the nanoparticle, the reflectance is higher in the samples of the ventilated façade serving as a substrate compared to the acrylic substrate.

Concerning the colourimetric parameters, Figure 18 represents the calculated colour difference and the Yellowness Index for the two systems with doped finishing coatings. The results showed that the SiO_2 nanoparticles have acceptable performance, as the ΔE is below 3. The exterior SIP samples also present better results for the SiO_2 nanoparticles. However, the validity of the results is questionable due to the high cracking of the coating, as already mentioned.

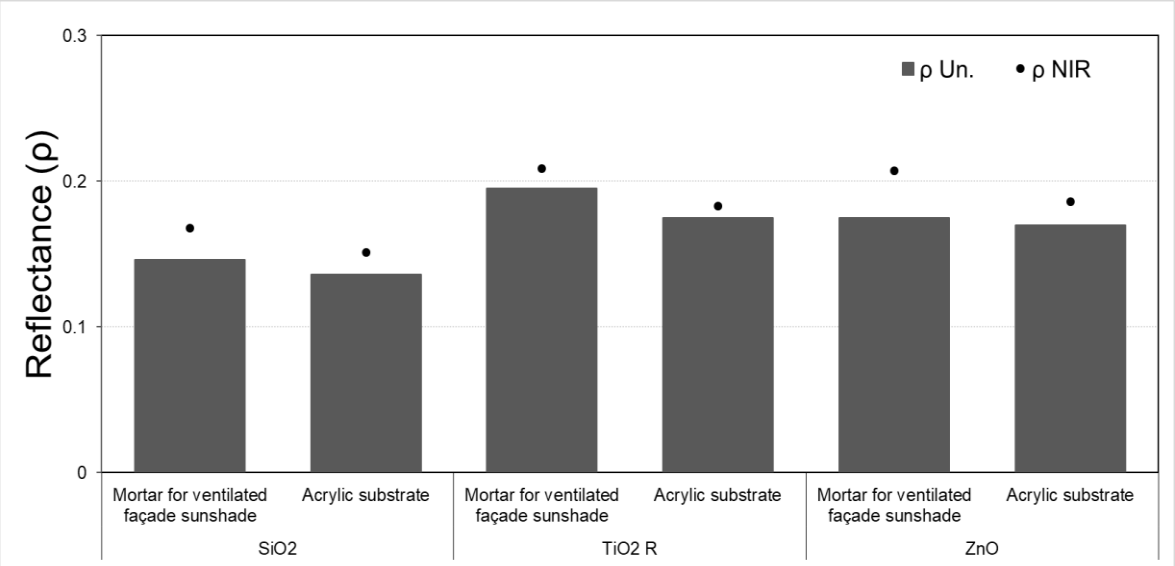

Figure 17: Comparison of total and NIR reflectance for the mortar of the ventilated façade panel and in acrylic substrates.

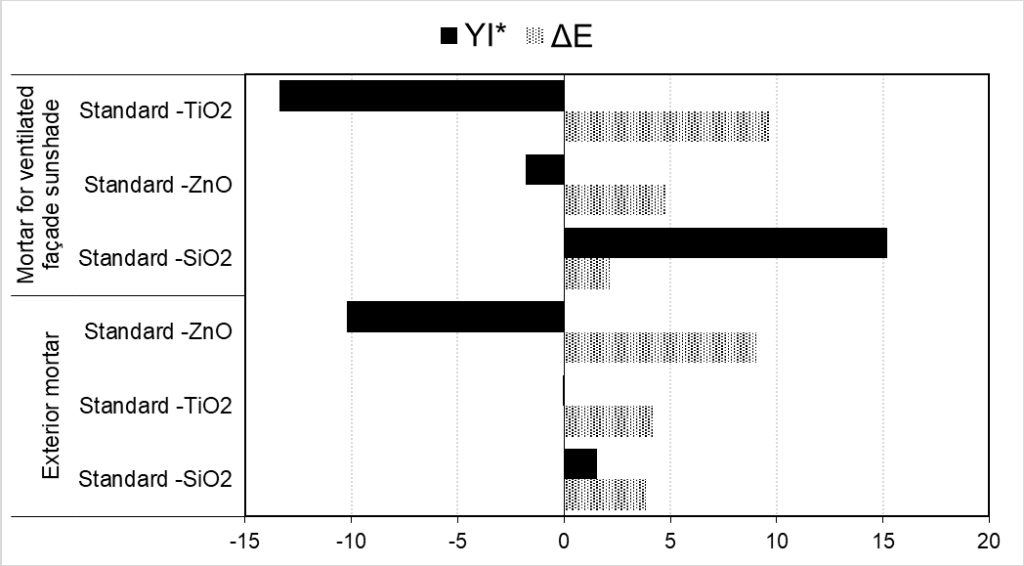

Figure 18: Color change of the SIP systems with acrylic paint.

The emissivity of a material surface is its effectiveness in emitting energy as thermal radiation. The emissivity measures were carried out using the standard procedures described in ASTM C1371, which conceals a technique for determining the emissivity of typical material near room temperature using a portable differential emissometer (Figure 19).

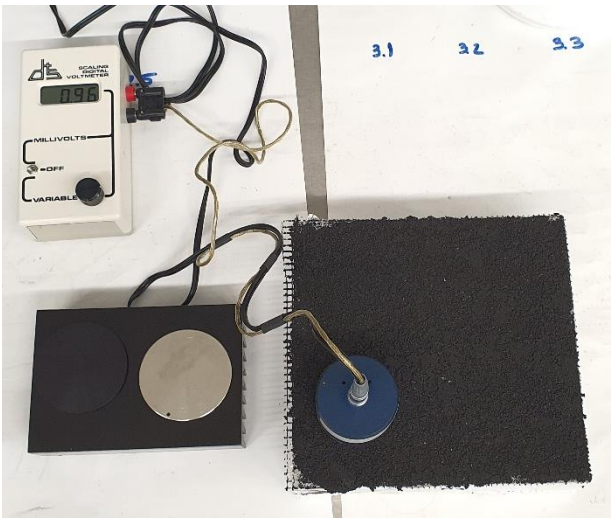

Figure 19: Portable differential emissometer apparatus.

When a consistent measure is obtained, it is possible to calculate the radiative heat flow from the surface. Knowing the surface (T1) and room temperature (T2), the radiative heat flow, given by the Stefan-Boltzmann Law [6], is described as:

$$q_r^n = \varepsilon \times \sigma \times (T_1^4 - T_2^4) \quad (6)$$

where σ is the Stephan-Boltzmann constant (5.6697×10^{-8} W/m^2 K^4), q_r^n is the amount of heat transferred by radiation, per unit area, in W/m^2, T is the temperature in Kelvin and ε is the emissivity. To simplify, we considered that the finishing coatings are opaque to infrared radiation (τ =0), as such, the energy balance is reduced to:

$$\varepsilon_\lambda = 1 - \rho_\lambda \text{ if } \tau = 0$$

$$\alpha_\lambda = \varepsilon_\lambda$$

By measuring the emissivity, it is possible to quantify the amount of long-wave electromagnetic radiation that a body emits, on which the body's surface temperature is dependent. Thus, their values can vary from 0 to 1, with high emissivity values related to lower temperatures. The experimental emissivity values of the SIP panels are represented in Table 6.

Table 6: Experimental emissivity values of SIP panels.

System	With/Without finishing coating	Sample	Average emissivity ($\varepsilon_{ave.}$)
SIP – Exterior mortar	Without	Argamassa Padrão – Sem revestimento	0.87
	With	SiO_2	0.82
		TiO_2	0.91
		ZnO	0.92
		Standard Acrylic paint	0.93
SIP – mortar for ventilated facade panel	With	SiO_2	0.80
		ZnO	0.82
		TiO_2 R	0.79
		Standard Acrylic paint	0.83

The emissivity results are similar within the same system and when analysed between the two systems. Although, it is possible to conclude from the values that the SiO_2 nanoparticles impose a decrease in the emissivity of the exterior plaster of the SIP. On the other hand, the ZnO nanoparticle led to an increase for both SIP systems.

7. Durability assessment

7.1. Core panels production

To carry out the durability tests, 40×40×15 cm panels were produced, constituting the core. Formulation 47 was selected as the most promising material considering its physicomechanical properties. To this end, we divided the panel into two layers to cure it in the best possible way.

We started by mixing the precursors with the activators (sodium hydroxide - 3 molal - and sodium silicate), with the help of a mixing machine (for approximately 30 min), then placing them in a climatic chamber, with the conditions of 85ºC/40% humidity.

This first layer was 7 cm thick (as we can see in the following Figure 20). After 4 hours (after the start of curing), the second layer was placed under the same temperature and humidity conditions. Then, the sides were removed (8 hours after the start of curing) so that the specimen could cure homogeneously due to its contact surface.

a) b)

Figure 20: (a) Placement of the first layer and (b) Removal of the sides.

Finally, the panels were removed from the climatic chamber after completing 20 hours of curing.

7.2. Preparation and assembly of the new panels

7.2.1. Panel configurations

Three different panel configurations were produced to assess the durability considering the developed and tested materials presented in the previous chapters, as shown in Table 7 and Figure 21.

Table 7: Constitution of the panels for the durability assessment.

Reference	Core formulation	External rendering system		Number and dimension of the specimens
		On top of OSB	Finishing coating	
Ref. 1	47 (15 cm thickness)	Commercial basecoat	Acrylic paint	4 samples (40 x 40 cm^2)
Ref. 2			Acrylic paint doped with nanoparticles	
Ref. 3			-	

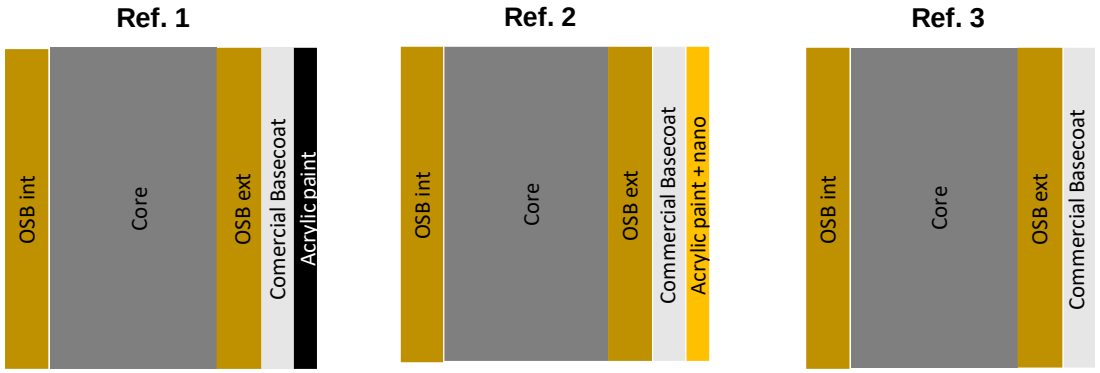

Figure 21: Schematic representation of the panel configurations

7.2.2.Core panel preparation

All the core panels produced in UTAD required initial surface treatment to achieve the defined flatness and geometry, as can be seen in Figure 22. As such, all the core panel surfaces were machined (see Figure 23).

Figure 22: Core surface before treatment

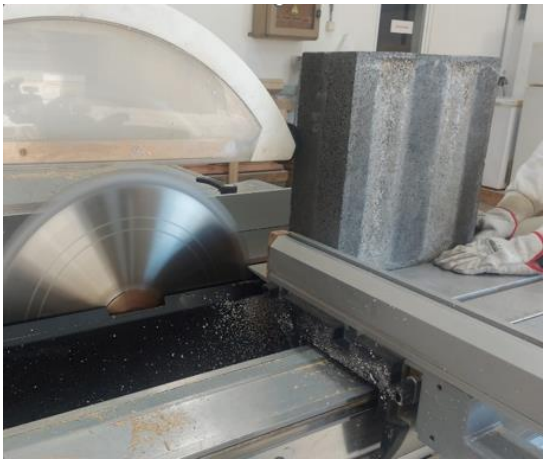

a) b)

Figure 23: a) Surface cutting; b) Core panel after treatment.

7.2.3.Production of Reference 1

The core panel was assembled to the OSB slab (previously cut to the required dimensions) using polyurethane glue, which is used to produce traditional SIP panels. Then, a reinforced commercial basecoat was applied on top of the OSB slab, covered with a primer and finished with black acrylic paint (see Figure 24 and Figure 25).

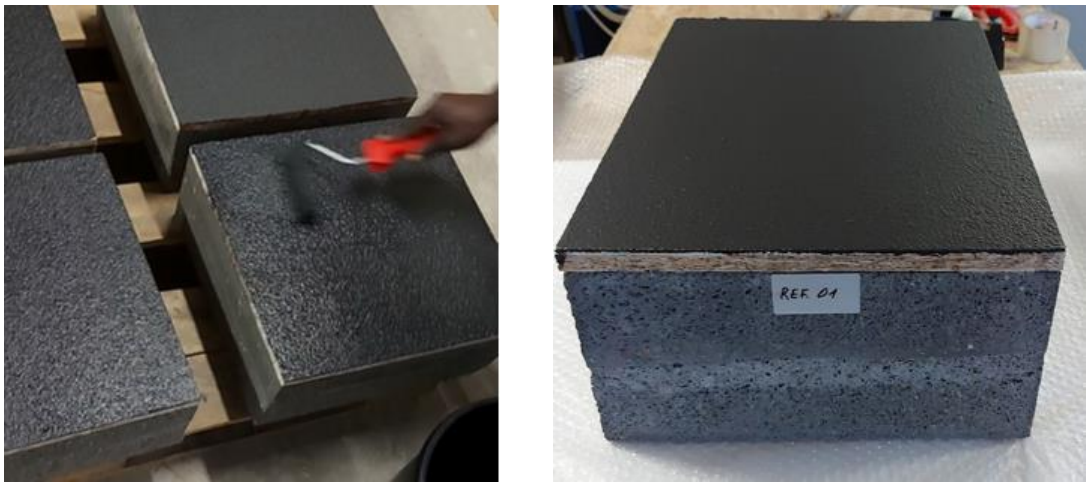

a) b)

Figure 24: a) Acrylic paint application; b) Finished panel – Reference 1.

Figure 25: Panel constitution – Reference 1

7.2.4.Production of Reference 2

The production of the second configuration (Reference 2) followed the same procedures as Reference 1, excepting the black acrylic paint, which was doped with nanoparticles (see Figure 26 and Figure 27).

a) b) c)

Figure 26: a) Nanoparticles weighing; b) Incorporation of nanoparticles in the acrylic paint; c) Manual mixing.

a) b)

Figure 27: a) Doped acrylic paint application; b) Finished panel – Reference 2.

7.2.5.Production of Reference 3

The production of the third configuration (Reference 3) followed the same procedures as Reference 1, except the black acrylic paint, which was not applied, being the primer as outer layer (Figure 28).

Figure 28: Finished panel – Reference 3.

7.2.6.Main remarks

The cutting process evidence the need to use thick samples (above 4 cm) since the selected formulation is lightweight, which led to lower mechanical resistance. As such, the panels for the ventilated façade (with 2 cm) crack during this process. Also, it was not possible to use the press machine to assemble the core to the OSB panels. The alternative was to glue the panels using the weight of the core.

Incorporating the nanoparticles in the acrylic paint was also challenging to achieve a homogeneous dispersion. Despite this, the problem was overcome and the samples were painted without constraints.

After the curing period, the panels were carefully packed, as shown in Figure 29, to be sent and tested in SINTEF facilities.

Figure 29: Samples' packaging.

7.3. Accelerated ageing tests

7.3.1. Experimental method

The durability of building components can be assessed through long-term natural outdoor climate exposure or appropriate accelerated climate ageing in the laboratory. Several apparatuses can be used in laboratories to subject test samples to various climate exposures with different ageing methods and standards. We performed artificial climatic ageing tests in SINTEF's climate simulator, according to the Nordtest method NT Build 495:2000. This test was developed by SINTEF about 50 years ago. The method description was designed and later approved as the Nordtest method after many years of experience, including comparisons with natural climatic ageing of façade materials. The objective of the accelerated climate ageing tests was to define the durability of specific variants of the SIP qualitatively.

The samples were subjected to accelerated ageing for 1 month, corresponding to about 1 year of natural outdoor climate exposure. Note that the performed tests are not usually run to estimate the service life expressed in terms of the number of years, as their main purpose is to compare the ageing properties of different materials and components.

The results from the tests performed in the climate simulator include information on the changes occurring during the analysed period, the scale of such changes and the time of occurrence. The main findings are, therefore, qualitative and based on the fact that a change in the performance properties of the samples corresponds to a change in their appearance during the test. This includes, for instance, signs of degradation, such as cracks, loss of gloss, or delamination.

SINTEF's climate simulator is a non-commercial accelerated climate ageing apparatus where test samples are subjected by rotation to four different climate zones, as shown in Figure 30.

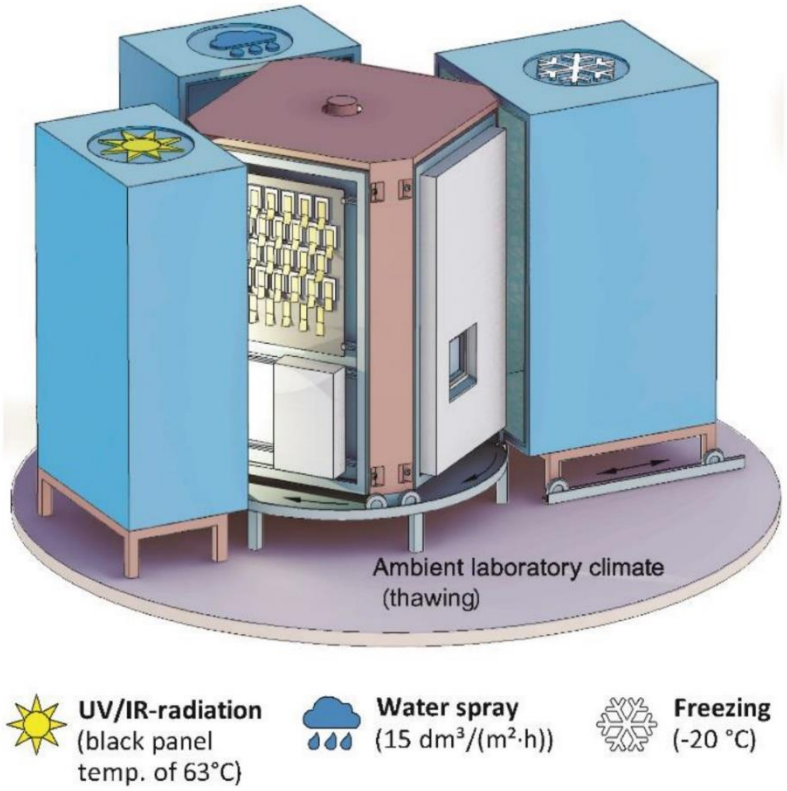

Figure 30: Climate simulator at SINTEF's laboratory

The first zone is an Ultraviolet (UV) and infrared (IR) irradiation chamber, where UV radiation is applied using fluorescent UV tubes with a relative spectral distribution in the UV band close to that of global solar irradiance. The black panel's temperature reaches a designated value (generally of 63 °C) in 45 minutes from UV light and heat radiation exposure. The black panel temperature may be chosen as 35±5 °C, 50±5 °C, or 75 ±5 °C, based on ISO 4892. The temperature is controlled using infrared halogen lamps and the UV intensity can vary at different levels depending on the choice of the UV tubes. For instance, for one specific set of UV tubes, the UVA and UVB intensities are averaged to 15 and 1.5 W/m^2, respectively.

The second zone is a water spray zone, where the specimens are wetted with a spray of demineralised water. The suggested strain is 15 dm^3/m^2/h, but several spraying conditions may be used. Furthermore, to allow water to drip off the examined samples, the spraying is terminated 10 min before the rotation into the third zone.

The third zone is a freezing zone, where an air temperature of -20±5 °C is suggested, but it is also possible to use other air temperatures if registered and reported.

The fourth and last zone is the ambient laboratory thawing zone, where the specimens are thawed at the laboratory climate of 23±5 °C and 50%±10% relative humidity (RH).

The exposure time is 1 hour in each climate zone in the given sequence.

The samples were prepared by sealing all the faces except the front (see Figure 31, exposed to the climate simulator and the back with epoxy glue. The samples were positioned in one of the four test faces in the mid-section of the climate simulator. The test stopped after 30 days.

Figure 31: Samples before testing.

7.3.2.Results

The test revealed different performances of the surface treatment of the samples. Visual control during and after the test sequence revealed the results shown in Table 8, Figure 32 and Figure 33.

Table 8: Results from testing in the climate simulator.

	Configuration 1	Configuration 2	Configuration 3
Start. 11.11.22		09.12.22 Visible cracks in the front face observed in all the samples	02.12.22 Visible cracks in the front face observed in all the samples
End 11.12.22	No cracks or delamination observed	Delamination observed in areas close to the cracks	Delamination observed in areas close to the cracks

a) b) c)

Figure 32: Samples after ageing.

Figure 33: Surface cracking (primer) after ageing – Reference 3

8. Environmental assessment

A life cycle analysis was carried out for the environmental assessment, considering the energy costs and the material required for the production, transport and grinding of the pulp. For calculation purposes, the production of 1 m^2 of the panel was taken into account.

Regarding grinding, it was not considered since the supplier previously ground the necessary materials. Regarding the production of panels, expenses related to the mixing machine and curing in the climatic chamber for 20 hours were considered.

Regarding transport, a truck with 100 m^3 and 22 tons of capacity was considered, with an average consumption of 50 l/100 Km. The calculations were carried out for two trips (round trip).

9. Microstructural analysis

The selected formulations doped with SiO_2 60-70 nm nanoparticles size at 0.5% concentration were morphologically analysed with a High-Resolution Environmental Scanning Electron Microscope (HRSEM) with Secondary Electron (SE) and Electron Backscattered Diffraction (EBSD) analysis (Quanta 400 FEG ESEM/ EDAX Genesis X4M) using an acceleration voltage of 15 kV. Depending on the formulation, the SEM images were taken at 75×, 250×, 300×, 500×, 1000×, 5000× and 10000×. An energy dispersive X-ray (EDX) mapping analysis of the composition of such formulations was carried out with an EDAX PEGASUS X4M using an acceleration voltage of 15 kV. From the SE images (Figure 34), it is possible to observe that the samples have a very porous structure. Through the BSE micrographs (left images of Figure 34), we can verify the formulation compositions' heterogeneity due to the different residues used.

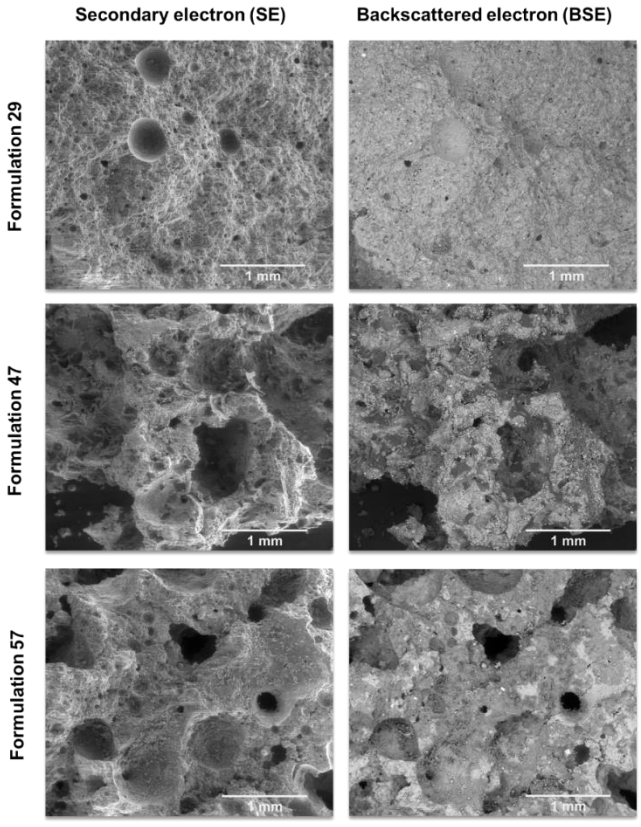

Figure 34: Secondary Electron (SE) and Electron Backscattered Diffraction (EBSD) analysis of the formulations doped with nanoparticles.

Formulation 29 has a porous structure with considerable heterogeneity in its composition, as shown in Figure 35. Using EDS analysis, it was possible to identify traces of

feldspar and marble from the waste used (EDX spectra from Z1 and Z2). We observed that the formulation presents sharp crystals of sodium hydroxide, revealing that the activators may not have reacted with the residues (EDX spectrum from the Z4 zone). Still, we could observe well-defined spherical particles from the fly ash.

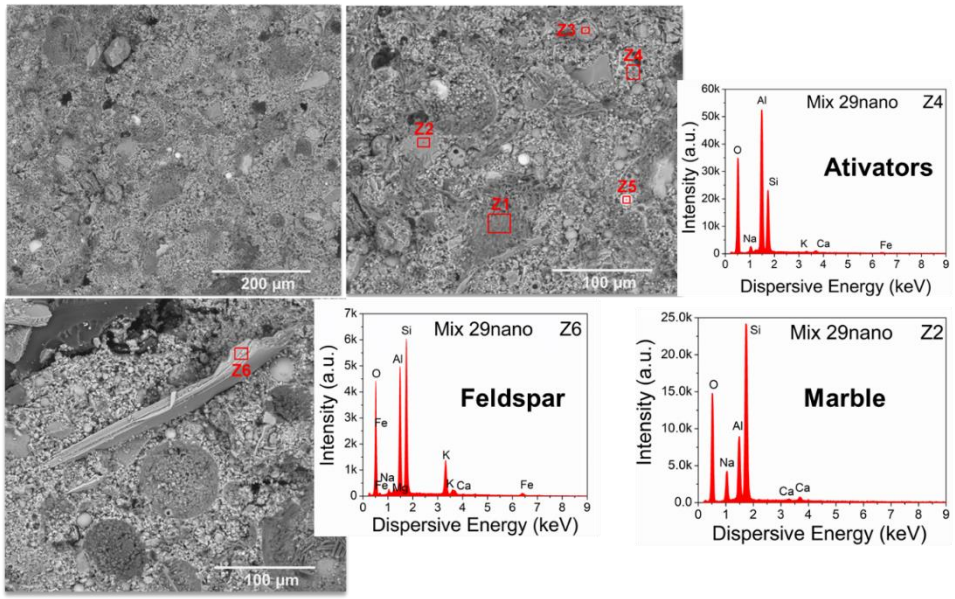

Figure 35: Scanning electron microscopy images of formulation 29 doped with nanoparticles. The EDX analysis is shown as insets.

In mixture 47 (Figure 36), it is also possible to observe a very porous structure. We detected organic structures from the timber (EDX spectrum corresponding to zone Z1) and a more flexible, typical polymeric structure, corresponding to the polyurethane used in the formation (EDX spectrum of zone Z2). It was also possible to observe crystallised sodium hydroxide, which may also indicate that the activators did not fully react with the residues. It can be noted that there is a large amount of fly ash with different sizes, represented by the perfect spherical shape, being constituted mainly by Fe and Mn.

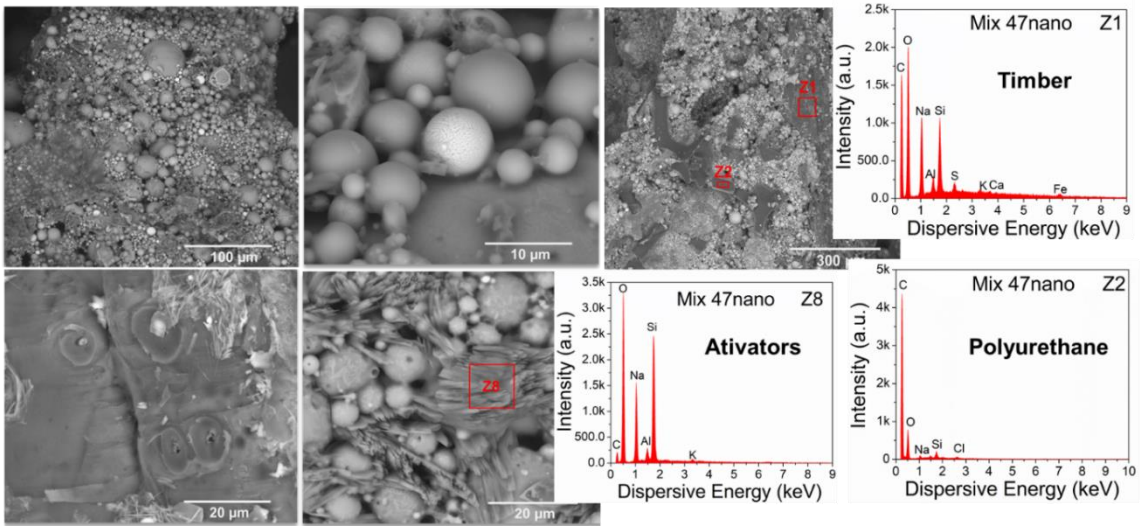

Figure 36: Scanning electron microscopy images of formulation 47 doped with nanoparticles. The EDX analysis is shown as insets.

In formulation 57 (Figure 37), noticeable sodium hydroxide crystals from alkaline activators. Larger silica particles and perfect spheres of aluminosilicates are detected (see the EDX analysis as insets). In this formulation, it was also possible to observe the incorporation of SiO_2 nanoparticles, with a highly ordered and reticulated structure, with a typical size of 30-60 nm.

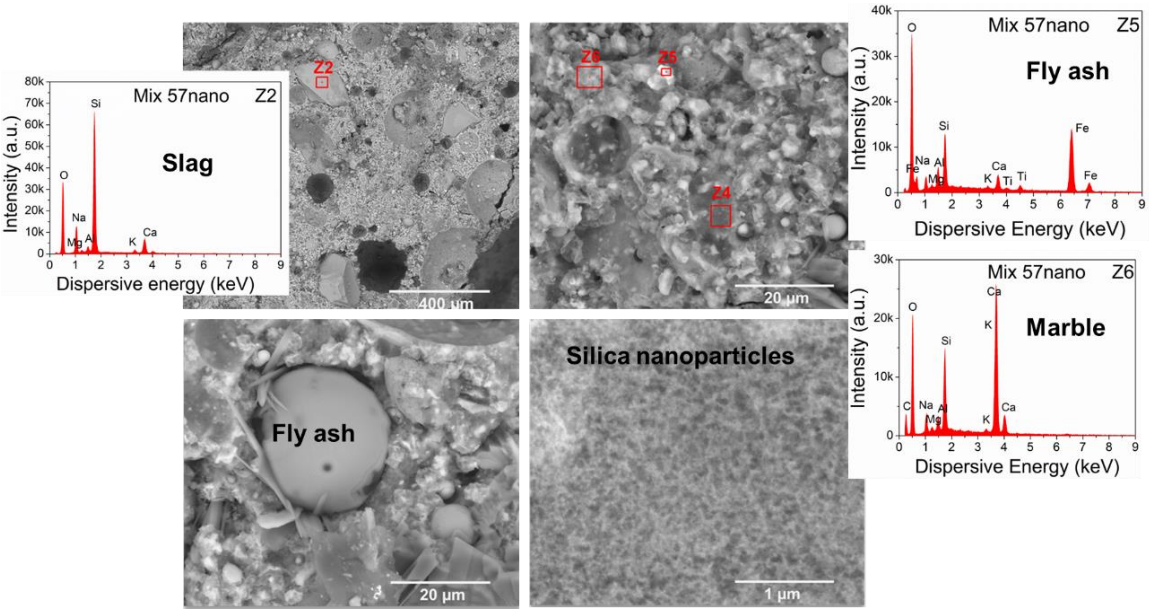

Figure 37: Scanning electron microscopy images of formulation 57 doped with nanoparticles. The EDX analysis is shown as insets.

Since the formulations were different in terms of composition, the EDX elemental maps for C, O, Na, Mg, Si, Al, P, S, Cl, K, Ca, Ti and Fe of the cross-section of the pastes were performed and are displayed in Figure 38, Figure 39 and Figure 40.

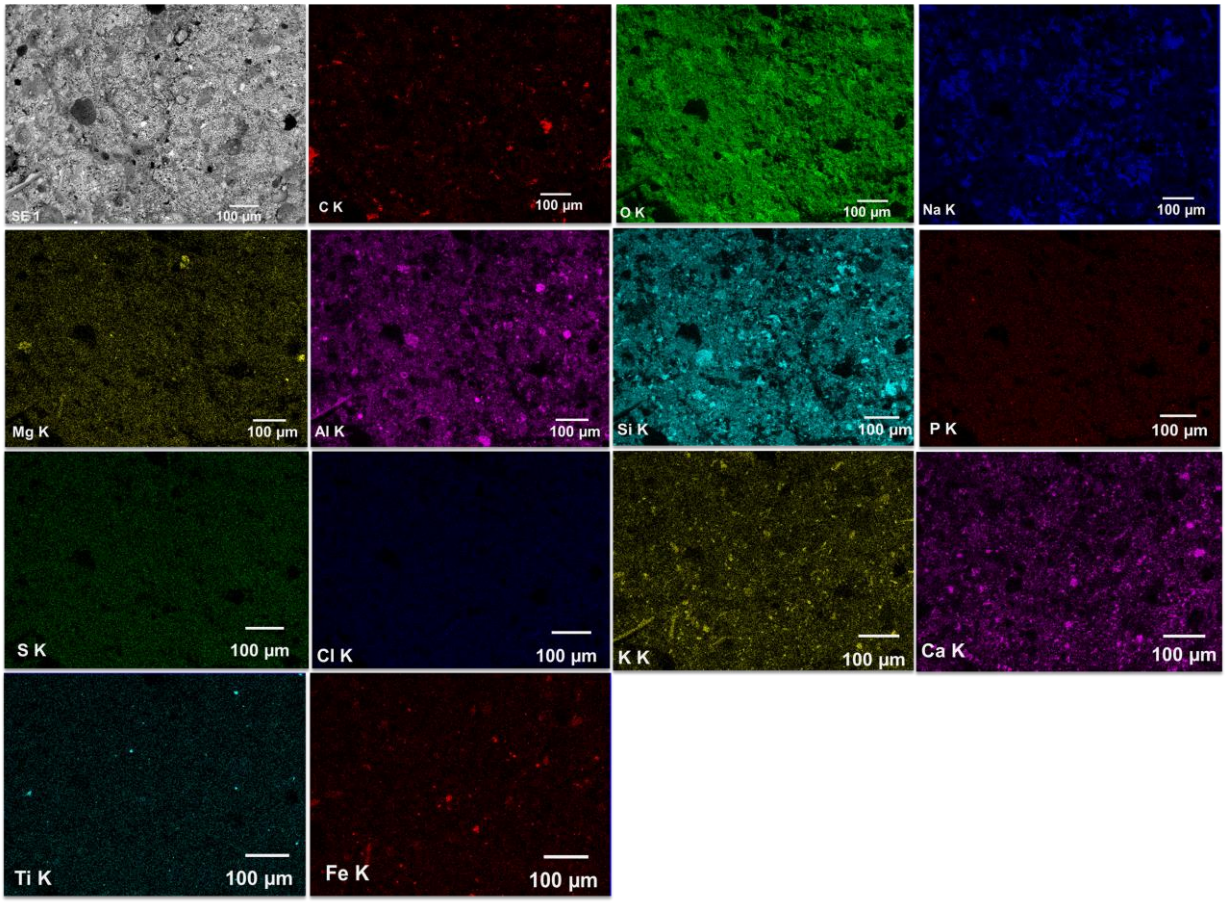

Figure 38: Energy dispersive X-ray spectroscopy (EDS) mapping composition of formulation 29 doped with SiO_2 60-70 nm nanoparticles.

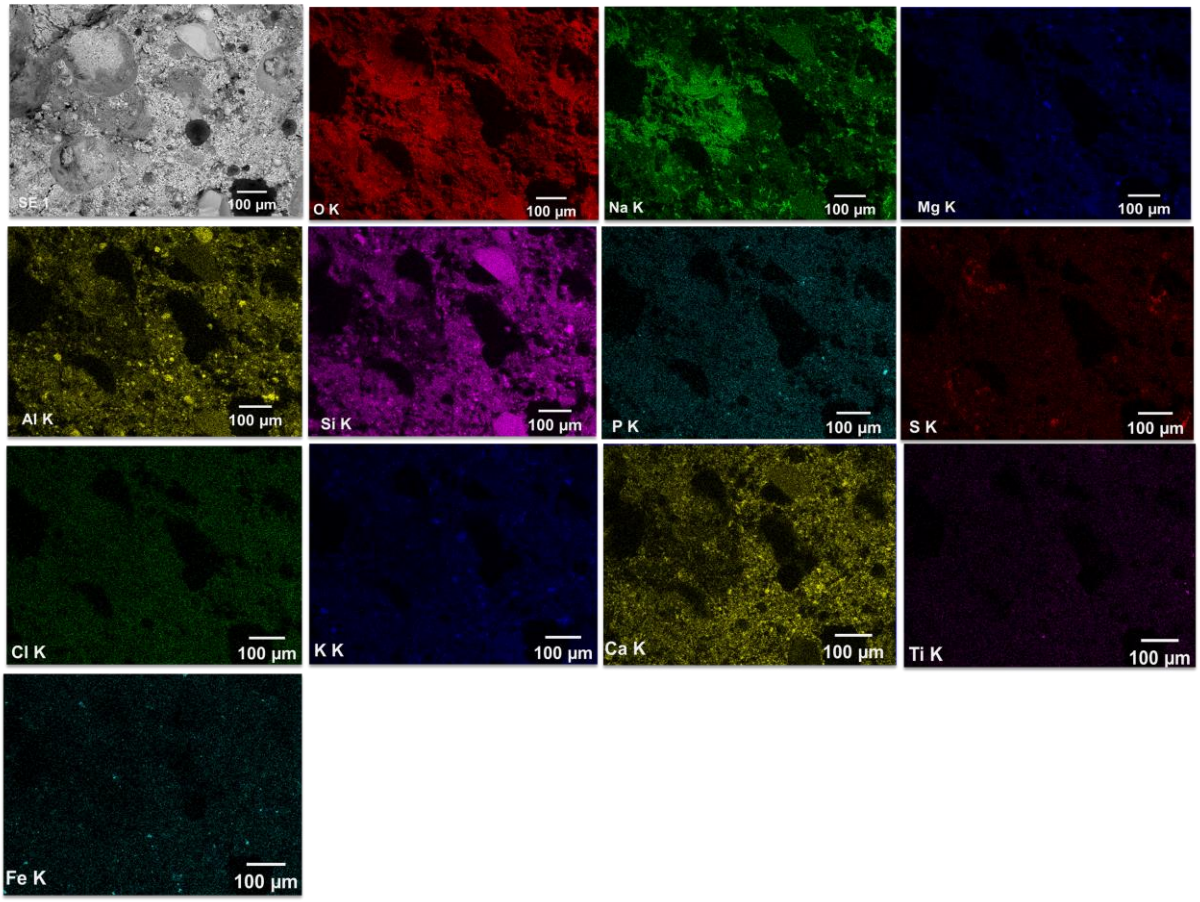

Figure 39: Energy dispersive X-ray spectroscopy (EDS) mapping composition of formulation 57 doped with SiO_2 60-70 nm nanoparticles.

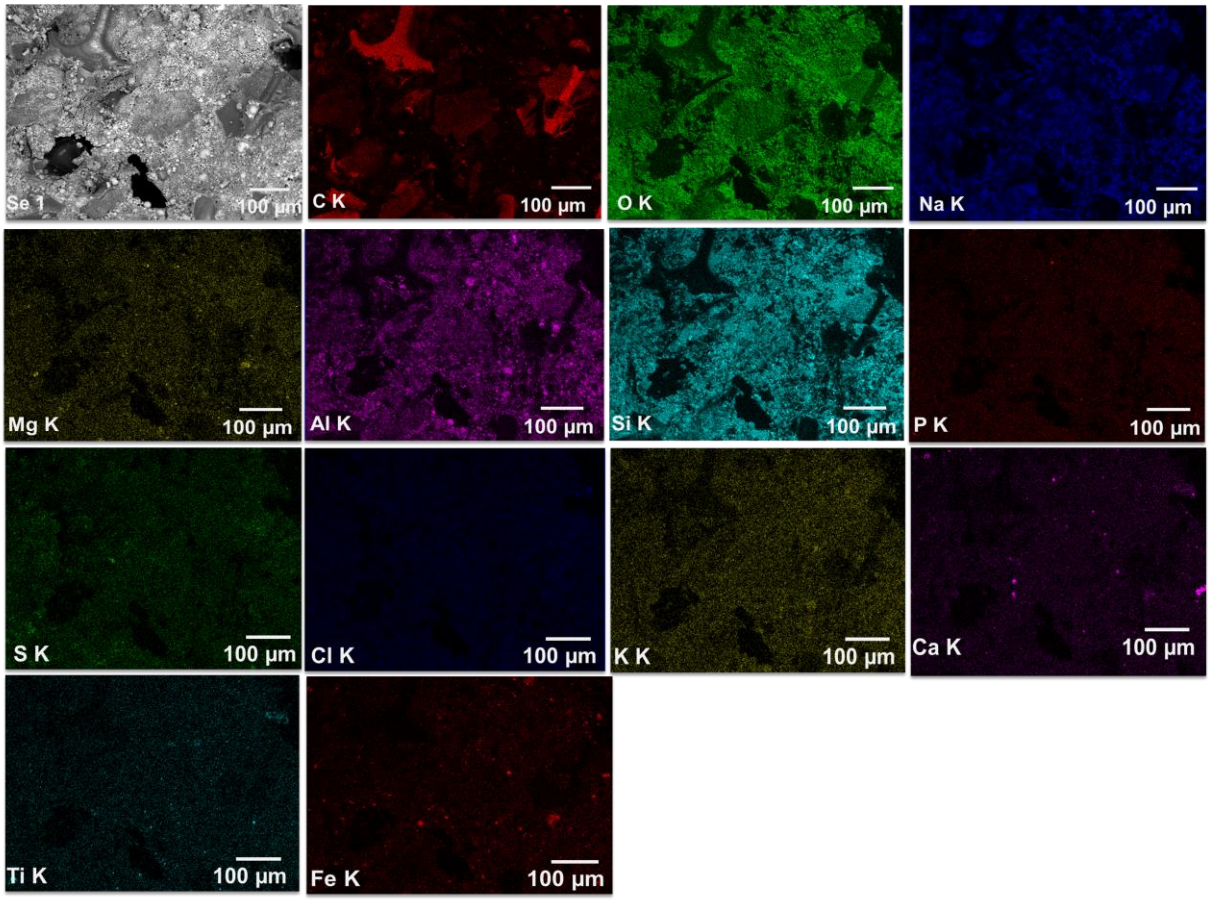

Figure 40: Energy dispersive X-ray spectroscopy (EDS) mapping composition of formulation 47 doped with SiO_2 60-70 nm nanoparticles.